CrystEngComm

Accepted Manuscript

This is an *Accepted Manuscript*, which has been through the Royal Society of Chemistry peer review process and has been accepted for publication.

Accepted Manuscripts are published online shortly after acceptance, before technical editing, formatting and proof reading. Using this free service, authors can make their results available to the community, in citable form, before we publish the edited article. We will replace this *Accepted Manuscript* with the edited and formatted *Advance Article* as soon as it is available.

You can find more information about *Accepted Manuscripts* in the Information for Authors.

Please note that technical editing may introduce minor changes to the text and/or graphics, which may alter content. The journal's standard Terms & Conditions and the Ethical guidelines still apply. In no event shall the Royal Society of Chemistry be held responsible for any errors or omissions in this *Accepted Manuscript* or any consequences arising from the use of any information it contains.

ROYAL SOCIETY OF CHEMISTRY

www.rsc.org/crystengcomm

TiO_2-B Nanoribbons Anchored with NiO Nanosheets as Hybrid Anode Materials for Rechargeable Lithium ion Batteries

Jiayan Zhang [a], Jianxing Shen [a]*, Tailin Wang [b], Huayong Zhang [a], Changbao Wei [a], Kechang Zhang [a], Yuanzheng Yue [c]

[a] Key Laboratory of Processing and Testing Technology of Glass & Functional Ceramics of Shandong Province, Qilu University of Technology, Jinan, 250353, China.

[b] State Key Laboratory of Crystal Materials, Shandong University, Shandanan Road, Jinan, 250100, China.

[c] Section of Chemistry, Aalborg University, Aalborg, DK-9000, Denmark

Abstract

A new type of TiO_2-B nanoribbons anchored with NiO nanosheets (TiO_2@NiO) is synthesized via a hydrothermal process and subsequent homogeneous precipitation method. XRD analysis indicates that TiO_2-B and cubic NiO phases exist in the composites. According to SEM images, the morphology of TiO_2@NiO hybrid material is unique, similar to that of leaf mosaic in biological system. According to electrochemical investigations, the nanostructured hybrid material as anode exhibits superior initial charge/discharge capacity and capacity retentions. The initial discharge capacity of TiO_2@NiO hybrid nanostructure is 395 mAh•g^{-1}, and the capacity remain 380 mAh•g^{-1} after 50 charge/discharge cycles, which is about 96.2% capacity retentions and 7.8 % higher than that of pristine TiO_2-B nanoribbons.

Keywords: TiO_2-B nanoribbon; NiO nanosheet; Nanostructure; Anode material; Lithium ion battery

*Corresponding author. Tel.: +86 531 89631225; Fax: +86 531 89631227. E-mail address: sjx@qlu.edu.cn (J.X. Shen)

CrystEngComm Accepted Manuscript

1. Introduction

Recently, Ti-based materials have attracted much attention as promising Li-ion battery anode materials owing to their abundant mineral resources, low cost, high safety and high operating voltage range [1-3]. Among those titanium compounds, TiO_2–B has more open structure and higher theoretical capacity (335 $mAhg^{-1}$) than other Ti-based materials [4]. TiO_2-B nanostructure has channels, which may be used for accommodating more lithium ions than any other bulk material. Moreover, the volume change of TiO_2 is less than 4% as Li-ions are inserted into the electrodes. Thus, TiO_2-B has been widely investigated as high-performance anode materials [5, 6]. In the past years, great progress has been made in the preparation of NiO with different morphologies and structures [7-9]. At the same time, nickel oxides (NiO) have been widely investigated due to their potential applications in electrochromic films, sensor, electrochemical capacitors, photocatalysts, batteries, etc. [10-13]. Compared to TiO_2, NiO has a higher theoretical capacity, which is 718 $mAh•g^{-1}$ as anode material for the LIBs [14].

An et al. [15] synthesized titania nanotubes modified with NiO nanoparticles, and the nanostructure had a better electrochemical activity that is beneficial to the improvement of the high rate charge/discharge capability. Choi et al. [16] prepared core–shell-structured NiO@TiO_2 by one-pot flame spray pyrolysis from an aqueous spray solution containing Ni and Ti components. The NiO@TiO_2 nanopowder exhibits higher capacity and better capacity retention compared to the pure NiO nanopowder. In this paper, a new type of TiO_2@NiO hybrid nanostructure consisting

CrystEngComm Accepted Manuscript

of TiO_2 nanoribbon and NiO nanosheet was created by using a two-step wet-chemical process, i.e. homogeneous precipitation (HPM) combined with hydrothermal process. The resulting material has unique morphology and good electrochemical performance.

2. Experimental

All reagents used in this work were analytical grade and used without further purification. Solutions were freshly prepared with deionized water. Synthesis of TiO_2–B nanoribbon is described elsewhere [17].

2.1 Synthesis of TiO_2@NiO hybrid materials

TiO_2@NiO hybrid materials were prepared through a homogeneous precipitation method. The precursor solutions were obtained by dissolving 0.005 mol of $Ni(NO_3)_2$•$6H_2O$ into 50 ml distilled water. Then 0.05 g TiO_2 nanoribbons and 0.4 g carbamide were dispersed into the $Ni(NO_3)_2$ solution. Subsequently, the as-prepared solutions were hydrothermally treated at 120 ˚C for 4, 5, and 6 h respectively. The products were washed with deionized water and dried at 80 ˚C for 2 h, then heat-treated in furnace at 400 ˚C for 2 h to obtain TiO_2@NiO hybrid materials, which were marked as TiO_2@NiO-4h, TiO_2@NiO-5h, and TiO_2@NiO-6h, respectively.

2.2 Electrochemical characterization

The electrochemical performance was evaluated using a two-electrode coin-type cell (CR2025). The anode materials were prepared by mixing the as-prepared samples with acetylene black (conducting agent) and polyvinylidene fluoride (binder) in a weight ratio of 70:18:12. After being blended in N-methyl pyrrolidinone (NMP), the mixed slurry was spread uniformly on a thin copper foil and dried in vacuum for 12 h

CrystEngComm Accepted Manuscript

at 120 °C and cut into circular strips of 15 mm in diameter. The weight of active material is about 2 mg in each coin cell. The electrolyte was composed of a 1 M $LiPF_6$ dissolved in ethylene carbonate (EC)/ dimethyl carbonate (DMC)/ethylene methyl carbonate (EMC) with the volume ratio of 1:1:1. A metal lithium foil was used as the counter and reference electrode and a polypropylene micro-porous film was used as the separator. The assembly of the coin cells was carried out in a dry argon-filled glove box at room temperature.

All the electrochemical measurements were performed in the form of CR2025 coin cells. The charge-discharge tests of the cells were tested between 1.0 and 3.0V on a battery testing system BTS (Newarel Electronic Co., Ltd. China) at room temperature. After setting parameters, constant-current charge process, constant-voltage charge process and constant-current discharge process can be automatically realized. Rate performance of the electrodes was then carried out at different current densities. The cyclic voltammetry (CV) test was performed on a CHI630A (Chenhua Co., Ltd.China.) electrochemical workstation with a scan rate of 0.1 mV s^{-1} in a potential range of 1.0-3.0 V.

3. Results and discussion

3.1 X-ray diffraction analysis

CrystEngComm Accepted Manuscript

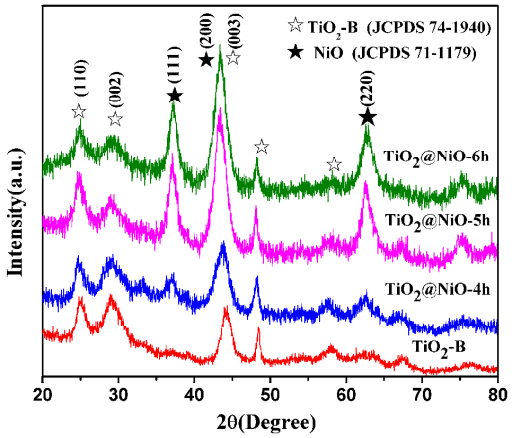

Fig. 1 XRD patterns of TiO_2-B nanoribbons and TiO_2@NiO hybrid materials.

Fig. 1 shows the XRD pattern of TiO_2-B nanoribbons and TiO_2@NiO hybrid materials. The diffraction peaks of TiO_2 obtained by calcining $H_2Ti_8O_{17}$ at 400 ˚C for 1 h can be indexed as TiO_2-B monoclinic structure (JCPDS file No.74-1940, C2/m), with lattice constants a=12.1787 Å, b=3.7412 Å, c=6.5249 Å and β=107.05°, and no characteristic peak is observed for other impurities such as rutile and anatase [18]. At the same time, Fig. 1 also presents the XRD patterns of the TiO_2@NiO hybrids prepared under different conditions (hydrothermal treatment time of 4, 5 and 6 h). Apart from the diffraction peaks of TiO_2-B, five diffraction peaks at 2θ = 37.245, 43.275 and 62.861° are clearly observed and can be indexed to the (111), (200), (220) of cubic structure of NiO, which represent the space group of Fm-3m (JCPDS file No.71-1179).

Reference Intensity Ratios (RIR) is used to quantify minerals in mixed mineral systems using powder XRD analysis. We also performed quantitative analysis on multi-phase patterns by means of RIR-quant analysis. The concentration of each phase is calculated by integrated intensity and RIR values. The RIR values of TiO_2-B

CrystEngComm Accepted Manuscript

and NiO are found to be 1.86 and 5.05 using Jade 5.0. We calculated the quality percentage of NiO according to the following equation

$$w_{NiO} = \frac{I_{NiO}}{I_{NiO} + \frac{I_{TiO_2}}{K_{NiO}^{TiO_2}}} \quad (1)$$

Where I_{NiO} is the peak intensity of NiO analyte phase, I_{TiO_2} is the peak intensity of TiO_2, and $K_{NiO}^{TiO_2}$ is the reference RIR values.

$$K_{NiO}^{TiO_2} = \frac{K_{Al_2O_3}^{TiO_2}}{K_{Al_2O_3}^{NiO}} = \frac{1.86}{5.05} \approx 0.368 \quad (2)$$

The calculated quality percentage of NiO is 11.505 (TiO_2@NiO-4h), 18.361 (TiO_2@NiO-5h) and 33.827 (TiO_2@NiO-6h), according to the formula described above. It is corresponding to the peak intensity of NiO.

3.2 Morphology analysis

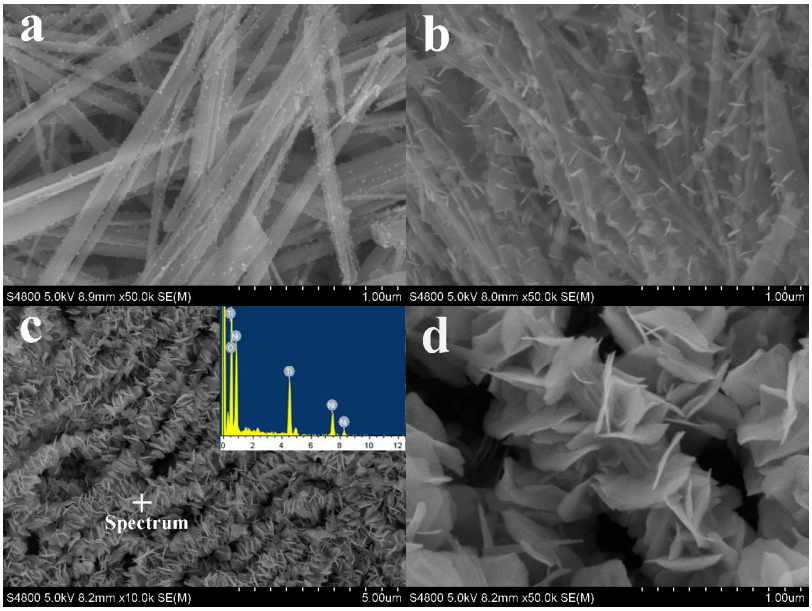

Fig. 2 SEM images of TiO_2@NiO hybrid materials
(a) SEM images of TiO_2@NiO-4h; (b) SEM images of TiO_2@NiO-5h; (c) SEM images of TiO_2@NiO-6h; (d) magnified SEM images of TiO_2@NiO-6h.

Fig. 2 shows the SEM images of the as-prepared TiO_2@NiO hybrid nanostructures.

CrystEngComm Accepted Manuscript

The morphology of TiO_2@NiO hybrid nanostructures is illustrated in Fig. 2a, revealing that NiO particle distributes uniformly on the TiO_2-B nanoribbons. When the hydrolysis time of urea was 5 h, abundant NiO nanoparticles or flocculent nanosheets were observed on the TiO_2-B nanoribbons (Fig. 2b). With increasing the hydrolysis time to 6 h, a large number of NiO nanosheets rather than NiO nanoparticles can be found on the surface of TiO_2-B nanoribbons (Figs. 2c and 2d), where the nanosheets are almost perpendicular to the TiO_2-B nanoribbons. This special shape of TiO_2-B nanoribbons anchored with NiO nanosheets is like the leaf mosaic in biology. The inset of Fig 2c displays the EDX analysis of the TiO_2@NiO hybrid nanostructures, indicating that the nanoribbons are composed of Ti, O, and Ni, with atomic percentage of 20.07 %, 49.37 %, 30.56 %, respectively.

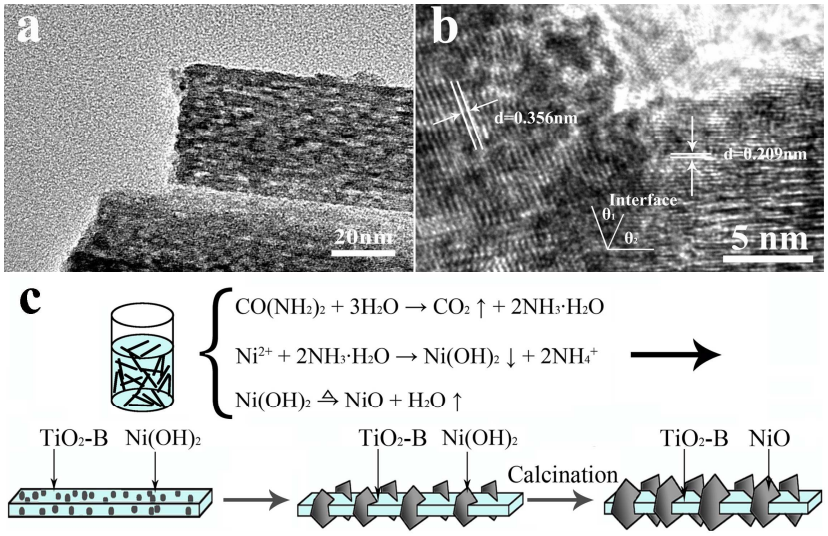

Fig. 3 HRTEM images of (a) TiO_2-B nanobelts and (b) TiO_2@NiO hybrid materials and (c) the Schematic sketch depicting the formation process of the TiO_2@NiO hybrid materials.

HRTEM images of TiO_2-B nanoribbons (Fig. 3a) show that the surface of TiO_2-B nanoribbons is coarse, and hence is energetically favorable for heterogeneous

CrystEngComm Accepted Manuscript

nucleation of NiO. The details of TiO_2@NiO nanostructures are shown in Fig. 3b. The lattice distance of TiO_2-B nanoribbons (d=0.356 nm) corresponds to the (110) planes of TiO_2-B, and the lattice distance of 0.209 nm is the typical (200) lattice plane of NiO. There is a clear interface between the nanosheets and the nanoribbons. In Fig 3b, θ_1=45.8°, which is the angle between the interface and (110) planes of TiO_2-B, the lattice distance of (110) is 0.356 nm, and hence the component perpendicular to interface is calculated to be 0.496 nm. In the same manner, θ_2 = 63.2°, the corresponding distance is 0.234 nm, almost half of TiO_2-B, the intimate contact between two planes is beneficial to combining TiO_2-B and NiO together and transportation of Li^+.

The formation mechanism of TiO_2@NiO hybrid materials is schematically illustrated in Fig. 3c. Based on our characterizations, we propose the following material growth mechanisms: First, TiO_2-B nanoribbon surface could offer preferred nucleation sites for heterogeneous nucleation of $Ni(OH)_2$. Small $Ni(OH)_2$ nanocrystalline nuclei tend to be anchored on the surfaces of nanoribbons due to the driving force of minimizing surface energy and then some $Ni(OH)_2$ nanoparticles were formed. With the increase of reaction time, the nanoparticles will continue to grow and eventually transform to nanosheets, which is a common morphology of $Ni(OH)_2$ under basic condition in the presence of urea. Moreover, surface area analysis was carried out by using the Brunauer-Emmett-Teller (BET) nitrogen adsorption method. The BET surface areas of $H_2Ti_8O_{17}$ nanoribbons, TiO_2-B nanoribbons, TiO_2@NiO-4h, TiO_2@NiO-5h and TiO_2@NiO-6h are measured to be

CrystEngComm Accepted Manuscript

37.6, 37.4, 42.5, 50.1 and 52.2 m^2g^{-1}, respectively. The value of TiO_2-B is similar to that of $H_2Ti_8O_{17}$, indicating that only the dehydration of $H_2Ti_8O_{17}$ occurs in the calcination process. With extending the HPM time, the BET surface area gradually increases, and the value of TiO_2@NiO-6h is increased by 39.6% compared to that of the TiO_2-B nanoribbons.

3.3 Electrochemical Performance

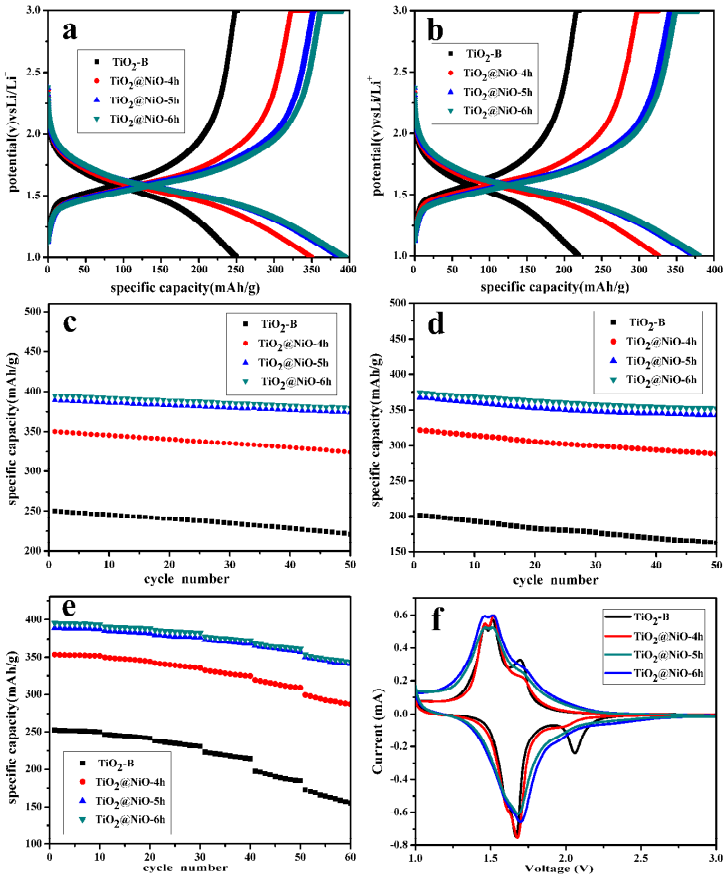

Fig. 4 The electrochemical performance of TiO_2-B nanoribbons and TiO_2@NiO hybrid materials (a) The initial charge/discharge curves of TiO_2-B nanoribbons and TiO_2@NiO at 0.5C; (b) The 50th charge/discharge curves of TiO_2-B nanoribbons and TiO_2@NiO at 0.5C; (c) The cycling performance of TiO_2-B nanoribbons and TiO_2@NiO at 0.5C; (d) The cycling performance of TiO_2-B nanoribbons and TiO_2@NiO at 5C; (e) The cycling performance of TiO_2-B nanoribbons and TiO_2@NiO at different charge/discharge rates; (f) The cyclic voltammetry curves of TiO_2-B nanoribbons and TiO_2@NiO.

CrystEngComm Accepted Manuscript

The initial galvanostatic charge/discharge curves measured at 0.5 C rates are shown in Fig. 4a. It is quite clear that the charge/discharge plateau of TiO_2-B nanoribbon is shorter than TiO_2@NiO hybrid materials, and the discharge capacity of TiO_2@NiO-6h is 394.8 mAh•g^{-1}. The coulombic efficiency for TiO_2-B nanoribbons, TiO_2@NiO-4h, TiO_2@NiO-5h and TiO_2@NiO-6h samples are 99.2, 98.8, 98.4, and 98.9%, respectively. The 50th galvanostatic charge/discharge curves measured at 0.5 C rates are shown in Fig. 4b. It can be seen that the discharge capacity of TiO_2-B nanoribbons is reduced to 221 mAh•g^{-1}, whereas the capacity of TiO_2@NiO-6h was still 380 mAh•g^{-1}. In comparison to the pristine TiO_2-B nanoribbon, the capacity retention of TiO_2@NiO-6h is 96.2 % and 7.8 % higher than TiO_2-B. At the same time, the coulombic efficiency for TiO_2@NiO-6h sample is 99.9%, showing better cycling performance compared to pristine TiO_2-B nanoribbon. The results clearly indicate that NiO nanosheet plays a significant role in improving the electrochemical performance of TiO_2-B nanoribbons.

The cycling behavior of bare TiO_2-B nanoribbons and TiO_2@NiO hybrid materials at 0.5 C and 5C is shown in Figs. 4c and d. In Fig. 4c (0.5C rate), after 50 cycles, the capacity retentions for the TiO_2-B nanoribbons, TiO_2@NiO-4h, TiO_2@NiO-5h and TiO_2@NiO-6h samples are 87.7, 93.2, 96.3 and 96.2%, respectively. In Fig. 4d (5C rate), After 50 cycles, the capacity retentions for the TiO_2-B nanoribbons, TiO_2@NiO-4h, TiO_2@NiO-5h and TiO_2@NiO-6h samples are 80.8, 89.7, 93.5 and 94.0%, respectively. Thus, TiO_2@NiO hybrid materials demonstrate higher capacity and cycling stability than pure TiO_2-B nanoribbons at both 0.5 and 5 C.

CrystEngComm Accepted Manuscript

The high capacity of the TiO_2@NiO hybrid materials is consistent with the high theory capacity (718 mAh•g^{-1}) of NiO [19]. NiO has a different Li^+ storage mechanism from that of TiO_2. The reaction of NiO with Li^+ is not an intercalation but a conversion process [20]: in the process of discharge NiO is transformed to elemental Ni. Just as the reaction (3); in the process of charge elemental Ni is transformed to NiO. Just as the reaction (4)

$$NiO + 2Li^+ + 2e^- \rightarrow Li_2O + Ni \quad (3)$$

$$Li_2O + Ni \rightarrow NiO + 2Li^+ + 2e^- \quad (4)$$

The formation of metallic Ni could improve the electrochemical performance of TiO_2@NiO hybrid materials by increasing the electrochemical activity of electrode [15]. Furthermore, TiO_2-B nanoribbons have a large surface area, and the introduced NiO has a flake structure, which further increases the BET surface area. The increased BET surface area increases the contact area between electrode and electrolyte, and provides the possibility of efficient transport of electrons and ions, which will lead to excellent electrochemical properties [21, 22]. The volume change of TiO_2 is less than 4% as Li-ions are inserted into the electrodes. The structure stability of TiO_2-B remains high after Li-ion insertion, and this is why the TiO_2@NiO hybrid materials have an extremely long cycling life [23]. What is more, according to Jang et al. [24] the interfacial kinetic resistance of the electrode decreases with an increase in surface area. Thus, TiO_2@NiO hybrid materials possess smaller interfacial kinetic resistance than TiO_2-B nanoribbons, and this is responsible for the excellent cycling stability of TiO_2@NiO hybrid materials.

CrystEngComm Accepted Manuscript

The cycling performance of the samples at different charge/discharge rates shown in Fig. 4e confirms the high rate capability and cycle stability of the as-prepared sample. Fig. 4f shows the cyclic voltammograms (CVs) of the samples. There are two pairs of cathodic/anodic peaks at around 1.6 and 1.7 V for the TiO_2-B nanoribbons, which are characteristic of Lithium insertion/deinsertion of TiO_2-B nanoribbons [25]. Another pair of peaks at around 1.7 and 2.0 V are assigned to the pseudo capacitive lithium storage behavior of TiO_2-B [26, 27], which are also exhibited in the curves of composite materials. Nevertheless, the peak intensity and integral areas of the TiO_2@NiO hybrid materials are different from those of TiO_2-B nanoribbons. TiO_2@NiO hybrid materials have larger integral areas and lower peak intensity, indicating their higher capacity and good cycle stability. These results are consistent with the galvanostatic charge/discharge measurements.

4. Conclusions

A new type of hybrid material containing 1D TiO_2 nanoribbons and 2D NiO nanosheets has been developed using a two-step wet-chemical method. The NiO nanosheets are anchored uniformly onto the nanoribbons and almost perpendicular to the TiO_2-B nanoribbons. The composite material reported here is a promising anode material for lithium ion batteries. TiO_2@NiO hybrid nanostructures exhibits higher charge/discharge capacity and capacity retentions after 50 cycles than TiO_2-B nanoribbons. Furthermore, TiO_2@NiO hybrid material could be further applied in other fields such as photocatalysis, solar cells, capacitors, and sensor due to its unique structure and performance.

CrystEngComm Accepted Manuscript

Acknowledgments

We express our appreciation for the financial support from the Science and Technology Foundation of Jinan, China (No. 201102056).

References:

[1] Shen, J.Y.; Wang, H.; Zhou, Y.; Ye, N.Q.; Wang, L.j. Continuous hollow TiO_2 structures with three-dimensional interconnected single crystals and large pore mesoporous shells for high-performance lithium-ion batteries. *CrystEngComm* 2012, 14, 6215-6220

[2] Xu, S.; Qin, Y.; Xu, C.; Wei, Y.; Yang, R.; Wang, Z.L. Self-powered nanowire devices. *Nat. Nanotechnol.* 2010, 5, 366–373.

[3] Nicholas, D.P.; Stephen, G. R.; Benjamin, E.W.; Anwesha, M.; Andreas, S. Control of TiO_2 Grain Size and Positioning in Three-Dimensionally Ordered Macroporous TiO_2/C Composite Anodes for Lithium Ion Batteries. *Inorg. Chem.* 2014, 53, 1100-1112.

[4] Andrew, S.D.; Anna, A.B.; Anton, V.V. Thermodynamics of Lithium in TiO_2(B) from First Principles. *Chem. Mater.* 2012, 24, 1568−1574.

[5] Anthony, G.D.; Graeme, H.; Keith J.S. Lithium Insertion in Nanostructured TiO_2(B) Architectures. *Acc. Chem. Res.* 2013, 46, 1104-1112

[6] Qu, J.; Wu, Q.; Ren, Y.; Su, Z.; Lai, C.; Ding, J. Enhanced High-Rate Performance of Double-Walled TiO_2-B Nanotubes as Anodes in Lithium-Ion Batteries. *Asian J. Chem.* 2012, 7, 2516–2518.

[7] Yu, W.; Jiang, X.; Ding, S.; Li, B. Preparation and electrochemical characteristics of porous hollow spheres of NiO nanosheets as electrodes of supercapacitors. *J. Power Sources* 2014, 256, 440-448.

CrystEngComm Accepted Manuscript

[8] Chen, X.; Zhang, N.; Sun, K. Facile ammonia-induced fabrication of nanoporous NiO films with enhanced lithium-storage properties. *Electrochem. Commun.* 2012, 20, 137–140

[9] Wang, X.; Li, X.; Sun, X.; Li, F.; Liu, Q.; Wang, Q.; He, D. Nanostructured NiO electrode for high rate Li-ion batteries. *J. Mater. Chem.* 2011, 21, 3571–3573.

[10] Patil, R.A.; Devan, R.S.; Lin, J.H.; Ma, Y.R.; Patil, P.S.; Liou, Y. Efficient electrochromic properties of high-density and large-area arrays of one-dimensional NiO nanorods. *Sol. Energy Mater. Sol. Cells* 2013, 112, 91–96

[11] Prasad, D.H.; Ji, H.I.; Kim, H.R.; Son, J.W.; Kim, B.K.; Lee, H.W.; Lee, J.H. Effect of nickel nano-particle sintering on methane reforming activity of Ni-CGO cermet anodes for internal steam reforming SOFCs. *Appl. Catal., B* 2011, 101, 531–539.

[12] Sun, W.; Chen, L.; Meng, S.; Wang, Y.; Li, H.; Han, Y.; Wei, N. Synthesis of NiO nanospheres with ultrasonic method for supercapacitors. *Mater. Sci. Semicond. Process.* 2014, 17, 129–133

[13] Li, J.; Meng, F.; Suri, S.; Ding, W.; Huang, F.; Wu, N. Photoelectrochemical performance enhanced by a nickel oxide–hematite p–n junction photoanode. *Chem. Commun.* 2012, 48, 8213–8215.

[14] Kavitha, T.; Yuvaraj, H. facile approach to the synthesis of high-quality NiO nanorods: electrochemical and antibacterial properties. *J. Mater. Chem.* 2011, 21, 15686–15691.

[15] An, L.P.; Gao, X.P.; Li, G.R.; Yan, T.Y.; Zhu, H.Y.; Shen, P.W. Electrochemical lithium storage of titania nanotubes modified with NiO nanoparticles. *Electrochim. Acta* 2008, 53, 4573–4579

CrystEngComm Accepted Manuscript

[16] Choi, S. H.; Lee, J.H.; Kang, Y.C. One-pot rapid synthesis of core–shell structured NiO@TiO_2 nanopowders and their excellent electrochemical properties as anode materials for lithium ion batteries. *Nanoscale* 2013, 5, 12645–12650.

[17] Zhang, J.; Shen, J.; Wang, T.; Wei, C.; Ma, Y.; Zhu, C.; Yue, Y. Improvement of capacity and cycling performance of spinel $LiMn_2O_4$ cathode materials with TiO_2-B nanobelts. *Electrochim. Acta* 2013, 111, 691–697

[18] Liu, S.; Jia, H.; Han, L.; Wang, J.; Gao, P.; Xu, D.; Yang, J.; Che, S. Nanosheet-Constructed Porous TiO_2–B for Advanced Lithium Ion Batteries. *Adv. Mater.* 2012, 24, 3201–3204.

[19] Yang, Z.K.; Song, L.X.; Xu, R.R.; Teng, Y.; Xia, J.; Zhao, L.; Wang, Q.S. Synthesis and lithium storage performance of nickel oxide octahedral. *CrystEngComm* 2014, 16, 9083-9089

[20] Hu, L.; Qu, B.; Chen, L.; Li, Q. Low-temperature preparation of ultrathin nanoflakes assembled tremella-like NiO hierarchical nanostructures for high-performance lithium-ion batteries. *Mater. Lett.* 2013, 108, 92–95.

[21] Shin, K.; Kim, H.J.; Choi, J.M.; Choi, Y.M.; Song, M.S.; Park, J.H. Controlled synthesis of skein shaped TiO_2–B nanotube cluster particles with outstanding rate capability. *Chem. Commun.* 2013, 49, 2326-2328

[22] Wang, C.; Zhou, Y.; Ge, M.; Xu, X.; Zhang, Z.; Jiang, J.Z. Large-Scale Synthesis of SnO_2 Nanosheets with High Lithium Storage Capacity. *J. Am. Chem. Soc.* 2010, 132, 46–47.

[23] Anthony G. D.; Graeme H.; Keith, J. S. Lithium Insertion in Nanostructured TiO_2(B) Architectures. *Acc. Chem. Res.* 2013, 46, 1104–1112.

CrystEngComm Accepted Manuscript

[24] Jang, H.; Suzuki, S.; Miyayama, M. Synthesis of open tunnel-structured TiO_2(B) by nanosheets processes and its electrode properties for Li-ion secondary batteries. *J. Power Sources* 2012, 203, 97–102.

[25] Chockla, A.M.; Klavetter, K.C.; Mullins, C.B.; Korgel, B. Solution-Grown Germanium Nanowire Anodes for Lithium-Ion Batteries. *ACS Appl. Mater. Interfaces* 2012, 4, 4658–4664.

[26] Wang, J.; Zhou, Y.; Shao, Z. Porous TiO_2(B)/anatase microspheres with hierarchical nano and microstructures for high-performance lithium-ion batteries. *Electrochim. Acta* 2013, 97, 386-392.

[27] Armstrong, A.R.; Armstrong, G.; Canales, J.; Garcia, R.; Bruce, P.G. Lithium-Ion Intercalation into TiO_2-B Nanowires. *Adv. Mater.* 2005, 17, 862–865.

CrystEngComm Accepted Manuscript

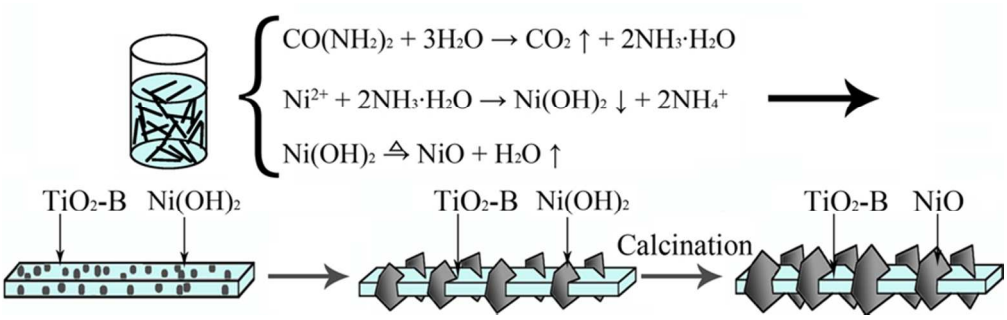

78x24mm (300 x 300 DPI)

CrystEngComm Accepted Manuscript